International Journal of Heat and Fluid Flow 62 (2016) 560–567

Contents lists available at ScienceDirect

International Journal of Heat and Fluid Flow

journal homepage: www.elsevier.com/locate/ijhff

Three-dimensional lattice Boltzmann simulation of suspensions containing both micro- and nanoparticles

A. Xu, T.S. Zhao*, L. Shi, X.H. Yan

Department of Mechanical and Aerospace Engineering, The Hong Kong University of Science and Technology, Clear Water Bay, Kowloon, Hong Kong SAR, China

ARTICLE INFO

Article history:
Available online 10 August 2016

Keywords:
Particle flows
Lattice Boltzmann method
Three dimension
Relative viscosity

ABSTRACT

In this paper, we present a three-dimensional lattice Boltzmann (LB) model to simulate suspensions that contain both micro- and nanoparticles. The microparticle dynamics is explicitly resolved by tracking individual solid particles, whilst the nanoparticles and base fluid are implicitly described as continua. The application of the LB model to simulate a micro spherical particle sedimentation in a microchannel and migration in a microtube filled with nanofluids show that the model allows the analysis of important parameters, including nanoparticle volume fraction, nanoparticle diameter, microchannel and microtube size. Finally, the model is applied to simulate particles in Couette flow. Through direct calculations of viscous dissipation, a mathematical correlation for viscosity as a function of micro- and nanoparticle volume fraction is proposed for the dilute suspension system.

1. Introduction

Suspended particles in fluid flows are ubiquitous in nature and play an important role in industries including mechanical engineering, chemical engineering, and biological engineering (Van der Hoef et al., 2008; Tenneti and Subramaniam, 2014). For example, to increase the energy density and volumetric capacity of redox flow batteries, one approach is to utilize the suspension electrode, which is composed of charge storing active materials, conductive additives, and an ion conducting electrolyte solution (Hatzell et al., 2015). The charge storing active materials are composed of particles with tens to hundreds of micrometers in diameter, while the conductive additives are particles with diameters ranging from tens to hundreds of nanometers. It is desirable to maximize the flows of all suspended particles at a minimum external pump power, thus, a thorough understanding of the hydrodynamics effect in a confined suspension is essential.

A number of studies have been conducted to gain an understanding of the particle transport mechanism. Feng et al. (1994a); 1994b) performed a particle-resolved simulation of circular particles settling in a two-dimensional channel flow where they identified Magnus lift, Saffman lift, and wall repulsion to be the dominant forces that propel particle migration. Dependence of particle migration trajectories on the particle Reynolds number was reported. Similarly, Jebakumar et al. (2016) reported the Stokes number effect on circular particle trajectories in a wall-bounded flow. In addition to spherical particles, Huang et al. (2012a); 2012b); 2014); Yang et al. (2015) simulated ellipsoid particles and investigated several rotational modes. To save the computational cost, Yang and Guo (2016) described the nanoparticle as a mass point to investigate its influence on binary fluid displacement; Zarghami et al. (2013) used two-fluid model to investigate flow and heat transfer in suspensions containing nanoparticles. In spite of extensive efforts, the understanding of particle transportation in confined suspension systems where particle diameters range from dozens of nanometers to hundreds of micrometers has yet to be comprehensive due to the multiple spatial scales.

Numerical approaches for studying suspensions are generally classified into three categories based on the levels of detail and accuracy required (Van der Hoef et al., 2008; Tenneti and Subramaniam, 2014). The first category is two-fluid approach, i.e., both solid and fluid phases are described as interpenetrating continua. The second category is point-particle approach, namely, the solid particle is treated as a discrete mass point and the fluid phase is considered as a continuum. In the point-particle approach, the drag closure is used for fluid-solid coupling. The third category is particle-resolved approach, i.e., fluid flow is solved by imposing appropriate boundary conditions at the particle surfaces, while the velocities and positions of the particles are determined by explicitly computing the fluid forces acting on the particles. The particle-resolved approach include the arbitrary Lagrangian–Eulerian (ALE) method Feng et al. (1994a; 1994b),

* Corresponding author. Tel.: +(852) 2358 8647.
E-mail address: metzhao@ust.hk (T.S. Zhao).

http://dx.doi.org/10.1016/j.ijheatfluidflow.2016.08.001
0142-727X/

immersed boundary (IB) method (Peskin, 1977), fictitious domain (FD) method (Glowinski et al., 2001), and lattice Boltzmann (LB) method (Ladd, 1994). Among these methods, the LB method has received much attention, primarily because the fluid-solid interface can be easily implemented in the regular Cartesian grids, thereby improving the computational efficiency for moving particle simulations. Specifically, the no-slip boundary condition can be achieved by modifications on the density distribution function encountering the surface. While the particle-resolved simulation is based on first-principle, the computational cost limits the suspension system that can be simulated. Thus, there is a trade-off between computational efforts and resolving down to a fine spatial and time scale.

In this work, we simulate a suspension that contains both micro- and nanoparticles by explicitly resolving microparticle dynamics and implicitly describing nanoparticles with base fluid as continua. The rest of the paper is organized as follows: In Section 2, we first present the three-dimensional multiple-relaxation-time LB model for simulating nanofluids, followed by particle-resolved LB model for simulating microparticle suspension. In Section 3, the present LB model is evaluated by verifying spherical sedimentation in a channel and migration in a tube. After that, numerical simulations are carried out to study microparticle motions in nanofluids, including the effects of nanoparticle volume fraction, nanoparticle diameter, and microparticle diameter to microchannel width ratio. Then, simulations are performed to study the viscous dissipation of particles in Couette flow. Based on the simulation data, a mathematical correlation for viscosity as a function of micro- and nanoparticle volume fraction is proposed for the dilute suspension system.

2. Numerical method

2.1. Single-phase method for nanoparticle suspension

2.1.1. The multiple-relaxation-time LB model

In single-phase method for nanofluids, the base fluid and the nanoparticles are assumed to be in equilibrium state. The influences of nanoparticles are reflected by changing physical properties of the mixture. The governing equation for nanofluids can be written as

$$\nabla \cdot \mathbf{u} = 0 \tag{1}$$

$$\frac{\partial \mathbf{u}}{\partial t} + \mathbf{u} \cdot \nabla \mathbf{u} = -\frac{1}{\rho_{\mathrm{nf}}} \nabla P + \nu_{\mathrm{nf}} \nabla^2 \mathbf{u} \tag{2}$$

where ρ_{nf} and ν_{nf} are the density and kinematic viscosity of nanofluids.

The evolution equation of LB model for fluid flow is written as

$$f_i(\mathbf{x} + \mathbf{e}_i \delta_t, t + \delta_t) - f_i(\mathbf{x}, t) = \Omega_i \tag{3}$$

where f_i is the density distribution function, t is the time, $\mathbf{x}$ is the fluid parcel position, $\mathbf{e}_i$ is the discrete velocity along the ith direction, δ_t is the time step, and Ω_i is the collision operator which can be expressed by either Bhatnagar–Gross–Krook (BGK) collision operator (Qian et al., 1992) or multiple-relaxation-time (MRT) collision operator (d'Humiéres, 2002; Lallemand and Luo, 2000). In this work, we adopt the MRT collision operator for its superior numerical stability over BGK collision operator. The MRT collision operator Ω_i is defined as

$$\Omega_i = -(\mathbf{M}^{-1}\mathbf{S}\mathbf{M})_{ij}\left[f_j(\mathbf{x}, t) - f_j^{\mathrm{eq}}(\mathbf{x}, t)\right] \tag{4}$$

For the three-dimensional D3Q19 lattice model, $\mathbf{e}_i$ can be given as

$$\begin{aligned}&\left[\mathbf{e}_0, \mathbf{e}_1, \mathbf{e}_2, \mathbf{e}_3, \mathbf{e}_4, \mathbf{e}_5, \mathbf{e}_6, \mathbf{e}_7, \mathbf{e}_8, \mathbf{e}_9, \mathbf{e}_{10}, \mathbf{e}_{11}, \mathbf{e}_{12}, \mathbf{e}_{13}, \mathbf{e}_{14}, \mathbf{e}_{15}, \mathbf{e}_{16}, \mathbf{e}_{17}, \mathbf{e}_{18}\right] \\ &= c\begin{bmatrix} 0 & 1 & -1 & 0 & 0 & 0 & 0 & 1 & -1 & 1 & -1 & 1 & -1 & 1 & -1 & 0 & 0 & 0 & 0 \\ 0 & 0 & 0 & 1 & -1 & 0 & 0 & 1 & 1 & -1 & -1 & 0 & 0 & 0 & 0 & 1 & -1 & 1 & -1 \\ 0 & 0 & 0 & 0 & 0 & 1 & -1 & 0 & 0 & 0 & 0 & 1 & 1 & -1 & -1 & 1 & 1 & -1 & -1 \end{bmatrix}\end{aligned} \tag{5}$$

where $c = \delta_x/\delta_t$ is lattice constant, and $c = 1$ is adopted in this work. $\mathbf{M}$ is a 19×19 orthogonal transformation matrix given by d'Humiéres d'Humiéres (2002). The relaxation matrix $\mathbf{S} = \mathrm{diag}(0, s_e, s_\epsilon, 0, s_q, 0, s_q, 0, s_q, s_\nu, s_\pi, s_\nu, s_\pi, s_\nu, s_\nu, s_\nu, s_t, s_t, s_t)$, where the relaxation parameters are given as $s_e = 1.19$, $s_\epsilon = s_\pi = 1.4$, $s_q = 1.2$, $s_t = 1.98$, and s_ν is determined by the kinematic viscosity of nanofluids.

The density distribution function f_i and its equilibrium distribution f_i^{eq} can be projected onto moment space via $\mathbf{m} = \mathbf{M}\mathbf{f}$ and $\mathbf{m}^{\mathrm{eq}} = \mathbf{M}\mathbf{f}^{\mathrm{eq}}$, respectively. Thus, the evolution equation of density distribution function can be rewritten as

$$\mathbf{m}^* = \mathbf{m} - \mathbf{S}(\mathbf{m} - \mathbf{m}^{\mathrm{eq}}) \tag{6}$$

where $\mathbf{I}$ is the unit tensor, and the equilibrium $\mathbf{m}^{\mathrm{eq}}$ is given by

$$\begin{aligned}\mathbf{m}^{\mathrm{eq}} = \rho_{\mathrm{nf}}\Big[&1,\ -11 + 19|\mathbf{u}|^2,\ 3 - \frac{11}{2}|\mathbf{u}|^2,\ u_x,\ -\frac{2}{3}u_x,\ u_y,\ -\frac{2}{3}u_y,\\ &u_z,\ -\frac{2}{3}u_z,\ 2u_x^2 - u_y^2 - u_z^2,\ -\frac{1}{2}(2u_x^2 - u_y^2 - u_z^2),\\ &u_y^2 - u_z^2,\ -\frac{1}{2}(u_y^2 - u_z^2),\ u_x u_y,\ u_y u_z,\ u_x u_z,\ 0,\ 0,\ 0\Big]^T\end{aligned} \tag{7}$$

The macroscopic density ρ_{nf} and velocity $\mathbf{u}$ are obtained from

$$\rho_{\mathrm{nf}} = \sum_{i=0}^{18} f_i, \quad \rho_{\mathrm{nf}}\mathbf{u} = \sum_{i=0}^{18} \mathbf{e}_i f_i \tag{8}$$

and the kinetic viscosity is given by

$$\nu_{\mathrm{nf}} = \frac{1}{3}c^2\left(\frac{1}{s_\nu} - \frac{1}{2}\right)\delta_t \tag{9}$$

2.1.2. Correlations of nanofluids

The density of nanofluids is calculated from Maiga et al. (2005); Oztop and Abu-Nada (2008)

$$\rho_{\mathrm{nf}} = (1 - \phi_{\mathrm{np}})\rho_{\mathrm{bf}} + \phi_{\mathrm{np}}\rho_{\mathrm{np}} \tag{10}$$

where the subscript nf, bf and np denote nanofluids, base fluid and nanoparticle, respectively. ϕ_{np} is the nanoparticle volume fraction.

Corcione (2011a); 2011b) presented a general correlation for viscosity of nanofluids based on experimental data (Das et al., 2003; He et al., 2007; Lee et al., 2008), which is written as

$$\frac{\mu_{\mathrm{nf}}}{\mu_{\mathrm{bf}}} = \left[1 - 34.87\left(\frac{d_{\mathrm{np}}}{d_{\mathrm{bf}}}\right)^{-0.3}\phi^{1.03}\right]^{-1} \tag{11}$$

where $d_{\mathrm{bf}} = 0.1\left[6M/(\pi N_A \rho_{f0})\right]^{1/3}$ is the equivalent diameter of a base fluid molecule, M is the molecular weight of the base fluid, and N_A is the Avogadro number. This correlation is applicable for nanoparticles diameter between 25 and 200 nm, volume fraction 0.01–7.1%.

2.2. Particle-resolved method for microparticle suspension

2.2.1. Translation and rotation of the microparticle

The solid microparticles are considered as rigid body, so the translational and rotational motion of the particles are determined by Newton's second law and Euler's second law, respectively:

$$M_{\mathrm{mp}}\frac{d\mathbf{U}(t)}{dt}=\mathbf{F}(t) \tag{12}$$

$$\mathbf{I}_{\mathrm{mp}}\cdot\frac{d\boldsymbol{\Omega}(t)}{dt}+\boldsymbol{\Omega}(t)\times[\mathbf{I}_{\mathrm{mp}}\cdot\boldsymbol{\Omega}(t)]=\mathbf{T}(t) \tag{13}$$

where the subscript mp denotes the microparticle, M_{mp} is the mass of the microparticle, and $\mathbf{F}$ is the force exerted on the particle. $\mathbf{I}_{\mathrm{mp}}$ is the inertial tensor of the microparticle, $\boldsymbol{\Omega}$ represents angular velocity and $\mathbf{T}$ is the torque exerted on the solid particle. For homogenous spherical particles, the nonlinear term $\boldsymbol{\Omega}(t)\times[\mathbf{I}_{\mathrm{mp}}\cdot\boldsymbol{\Omega}(t)]$ vanishes. Thus, a first-order Euler method for solving ordinary differential equations is applied at each time step to solve Eqs. 12 and 13.

2.2.2. Fluid-solid boundary interaction

At the particle's surface, the no-slip boundary condition should be guaranteed. Due to the fact that the simple bounce-back scheme requires an empirical correction for the effective hydrodynamic radius (Lishchuk et al., 2006), in this work, we adopt the interpolated bounce back scheme (Bouzidi et al., 2001; Lallemand and Luo, 2003) for accurate curve wall boundaries. The parameter $q=|\mathbf{x}_f-\mathbf{x}_w|/|\mathbf{x}_f-\mathbf{x}_b|$ is defined to describe the fraction in fluid region of a grid spacing intersected by the solid surface, where $\mathbf{x}_f$ is boundary fluid node, $\mathbf{x}_b$ is boundary solid node and $\mathbf{x}_w$ is solid boundary interface. Based on the relative location of $\mathbf{x}_w$, the interpolation scheme of the density distribution function after streaming is given as, for $q\le 0.5$

$$\begin{aligned}f_{\bar{i}}(\mathbf{x}_f,t)=\;&q(2q+1)f_i(\mathbf{x}_f+\mathbf{e}_i\delta_t,t)+(1-4q^2)f_i(\mathbf{x}_f,t)\\&-q(1-2q)f_i(\mathbf{x}_f-\mathbf{e}_i\delta_t,t)+2\omega_i\rho_0\frac{\mathbf{e}_{\bar{i}}\cdot\mathbf{u}_w}{c_s^2}\end{aligned} \tag{14}$$

for $q\ge 0.5$

$$\begin{aligned}f_{\bar{i}}(\mathbf{x}_f,t)=\;&\frac{1}{q(2q+1)}f_i(\mathbf{x}_f+\mathbf{e}_i\delta_t,t)+\frac{2q-1}{q}f_{\bar{i}}(\mathbf{x}_f-\mathbf{e}_i\delta_t,t)\\&-\frac{2q-1}{2q+1}f_{\bar{i}}(\mathbf{x}_f-2\mathbf{e}_i\delta_t,t)+\frac{1}{q(2q+1)}2\omega_i\rho_0\frac{\mathbf{e}_{\bar{i}}\cdot\mathbf{u}_w}{c_s^2}\end{aligned} \tag{15}$$

where $f_{\bar{i}}$ is the distribution function associated with the velocity $\mathbf{e}_{\bar{i}}=-\mathbf{e}_i$.

To calculate the force and torque exerted by the fluid on the solid particle, we adopt momentum-exchange method due to its simplicity and robustness. The hydrodynamic force acting on the solid surface is obtained by summing up the local momentum exchange of the fluid parcels during the bounce back process at the fluid solid interface over boundary links. Since the original momentum-exchange method proposed by Ladd (1994) lacks local Galilean invariance (Peng et al., 2016; Tao et al., 2016), in this work, we adopt the modified momentum-exchange method proposed by Chen et al. (2013), which uniformly distributes the momentum along the entire lattice link when accounting for the effect of covering fluid nodes or uncovering solid nodes.

The total force is calculated as

$$\mathbf{F}=\sum_{\mathbf{x}_f}\sum_{i_{bl}}\left\{\left[f_i^{+}(\mathbf{x}_f,t)+f_{\bar{i}}(\mathbf{x}_f,t+\delta_t)\right]\mathbf{e}_i-2\omega_i\rho_0\frac{\mathbf{e}_i\cdot\mathbf{u}_w}{c_s^2}\mathbf{u}_w\right\} \tag{16}$$

and the total torque is calculated as

$$\mathbf{T}=\sum_{\mathbf{x}_f}\sum_{i_{bl}}(\mathbf{x}_w-\mathbf{x}_c)\times\left[f_i^{+}(\mathbf{x}_f,t)(\mathbf{e}_i-\mathbf{u}_w)-f_{\bar{i}}(\mathbf{x}_f,t+\delta_t)(\mathbf{e}_{\bar{i}}-\mathbf{u}_w)\right] \tag{17}$$

where f_i^{+} denotes post-collision distribution function, and $\mathbf{x}_c$ is the center position of the solid microparticle. The double summations are first over the boundary links i_{bl} pointing from a given boundary node $\mathbf{x}_f$ into the solid surface, then over all the boundary nodes.

3. Simulation results and discussion

3.1. Validation I: Sedimentation of a sphere in a channel

We consider a spherical particle of diameter d released in a square channel of width L and then settled under gravity, as illustrated in Fig. 1(a). The terminal settling velocity of the particle is lower in an environment with finite walls than that in an unconfined domain. The wall effect is defined as $\xi=u_w/u_0$, where u_w is the terminal settling velocity of the particle in channel with nearby walls. The unconfined terminal velocity u_0 is calculated from the balance of gravity force, buoyancy force and drag force as

$$3\pi d\mu u_0=\frac{4}{3}\pi\left(\frac{d}{2}\right)^3(\rho_s-\rho_f)g \tag{18}$$

In the simulations, the channel width is set as $L=300$ μm. The density and dynamic viscosity of the liquid are $\rho_f=1$ g/cm^3 and $\mu=1$ g/(cm·s), respectively. The density of the solid particle is $\rho_s=2$ g/cm^3. Zero velocity is applied at the inlet, and the normal derivative of velocity is zero at the outlet. To save the computation cost, a moving computational domain proposed by Aidun et al. (1998) is used to mimic an infinitely long channel.

Fig. 1(b) shows the wall effects on particle settling velocity. Our LB simulation results using three different mesh sizes $N_x\times N_y\times N_z=40\times 40\times 120$, $60\times 60\times 180$, $80\times 80\times 240$ are compared with experimental data given by Miyamura *et al.* Miyamura et al. (1981). The two sets of results are in good agreement, demonstrating grid convergence of our adopted method.

3.2. Validation II: Migration of a sphere in a tube

We consider a neutrally buoyant spherical particle migrating in a tube, as illustrated in Fig. 2(a). The fluid flow is driven by the pressure difference at two ends of the tube. Initially, the particle is set off the center axis of the tube. Due to the Segré–Silberberg effect Segre (1961), the released particle will approach an equilibrium position roughly midway between the tube axis and the wall.

In the simulation, the particle center is initially set at $a/R=0.21$. The radii of the spherical particle and the tube are $r=0.375$ cm and $R=2.5$ cm, respectively. The dynamic viscosity of the liquid is $\mu=1$ g/(cm·s), and the density of the liquid is $\rho_f=1$ g/cm^3. The computational domain size is $327\times 109\times 109$ lattice. Pressure boundary conditions are set at the inlet and outlet. In the pressure driven tube flow, the maximum velocity in the axis of the tube is $U_m=\Delta pR^2/(4\mu L)$. The Reynolds number is defined as $Re=8r^2U_m/(\nu R)$, and the case of $Re=9$ is simulated to compare with results given by Yang et al. (2005). As shown in Table 1, the present simulation results agree well with that given by the arbitrary Lagrangian–Eulerian method and the fictitious domain method. From Fig. 2(b), we can see the Segré–Silberberg effect is reproduced.

3.3. A single microparticle settling in nanofluids

In suspensions containing micro- and nanoparticles, it is of engineering interest to determine how much drag force will increase

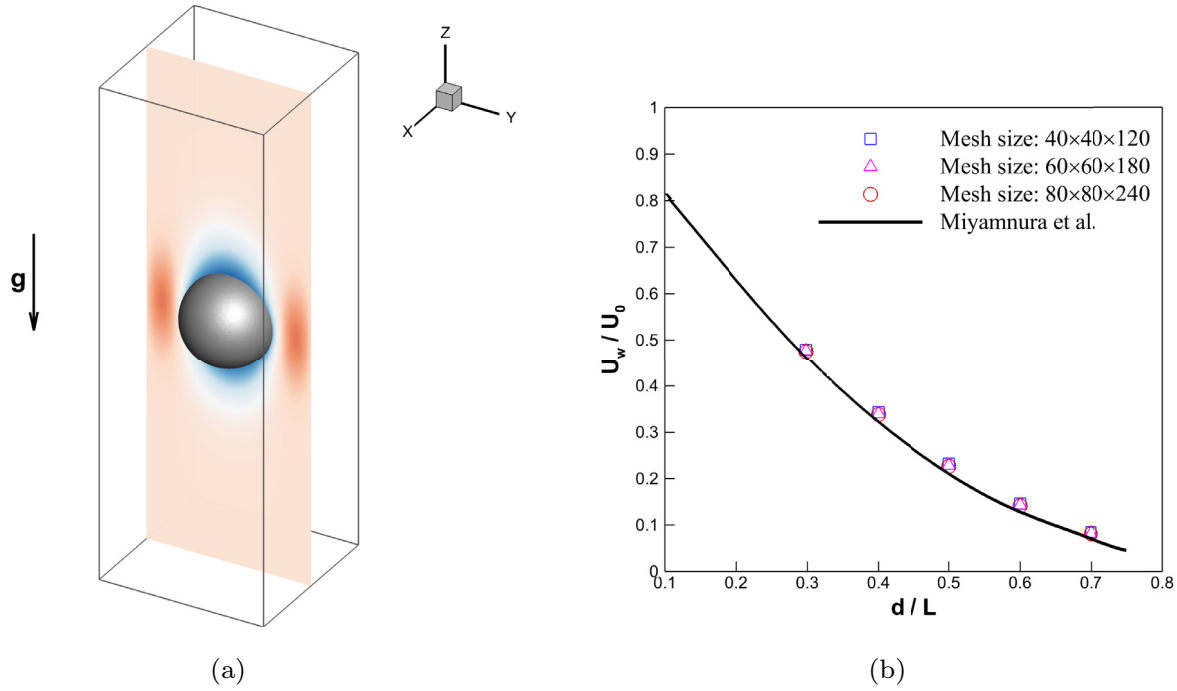

Fig. 1. A solid sphere particle settling in a channel under gravity: (a) illustration of computational setup, the slice shows velocity of liquid in vertical direction, (b) particle settling velocity under various particle diameter to channel width ratios.

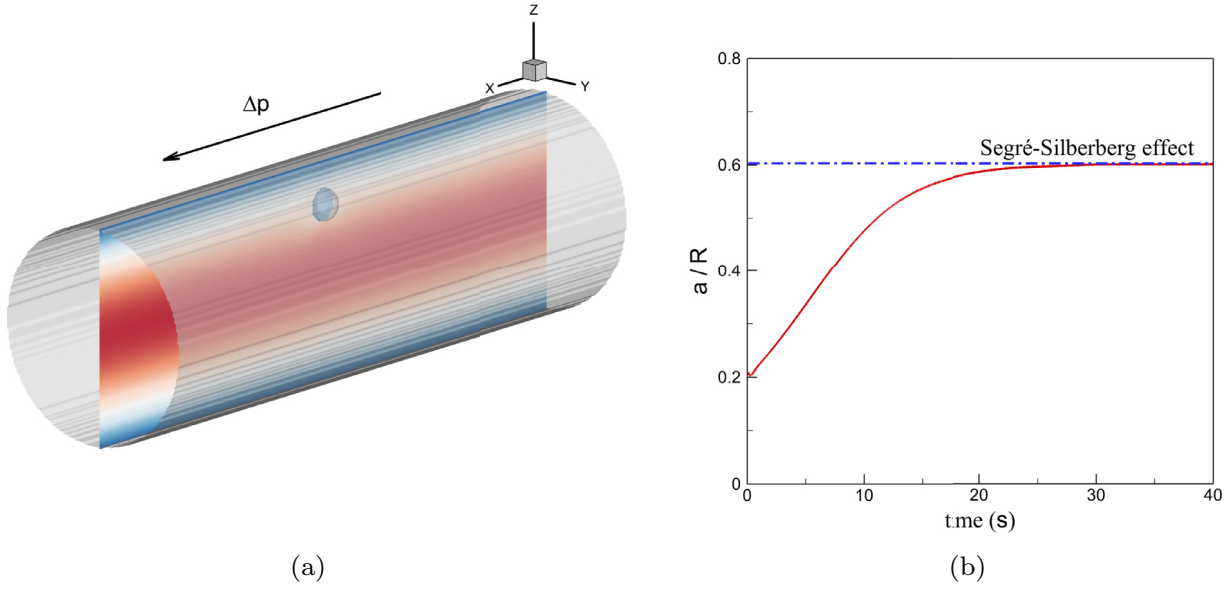

Fig. 2. A neutrally buoyant particle migrates in a pressure driven tube: (a) illustration of computational setup, the slice shows velocity of liquid in horizontal direction, (b) time history of particle center in radial direction.

Table 1
Equilibrium center position, horizontal velocity, and horizontal angular velocity of the particle .

	a/R	U_x	Ω_y
Present	0.602	12.3 cm/s	4.66 s^{-1}
Arbitrary Lagrangian–Eulerian method	0.601	12.4 cm/s	4.65 s^{-1}
Fictitious domain method	0.606	12.2 cm/s	4.63 s^{-1}

under various nanoparticle volume fraction and nanoparticle diameter. To evaluate the drag force of microparticle sedimentation in nanofluids, we calculated the drag coefficient C_d, which is defined as

$$C_d = \frac{F_d}{\frac{1}{2}\rho_{\mathrm{bf}} S U_t^2} = \frac{\frac{4}{3}\pi r_{\mathrm{mp}}^3 (\rho_{\mathrm{mp}} - \rho_{\mathrm{bf}}) g}{\frac{1}{2}\rho_{\mathrm{bf}} S U_t^2} \tag{19}$$

where F_d is the average drag force, U_t is the terminal settling velocity, and $S = \pi r_{\mathrm{mp}}^2$ is the projected area of the microparticle in the (x, y) plane.

In the simulations, the diameter of the microparticle is $d_{\mathrm{mp}} = 100$ μm, and the channel width is $L = 400$ μm. The density of the microparticle and nanoparticle are $\rho_{\mathrm{mp}} = 5$ g/cm^3 and

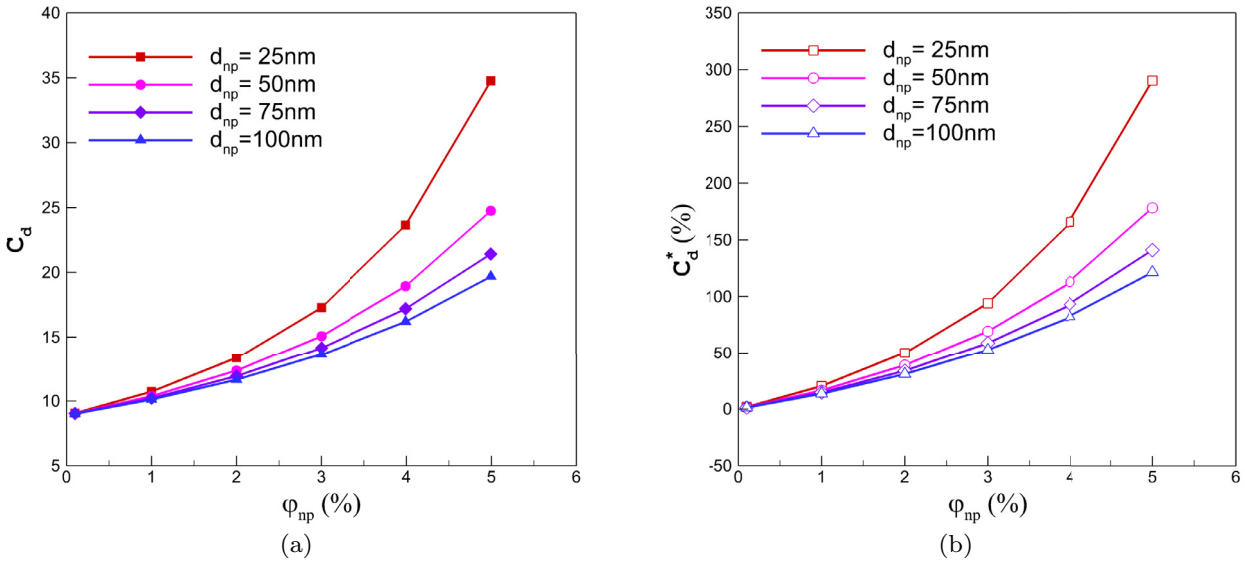

Fig. 3. Drag coefficient of a microparticle settling in nanofluids: (a) absolute values of drag coefficient, (b) relative values of drag coefficient compared without adding nanoparticles.

$\rho_{np} = 4$ g/cm^3, respectively. The density and dynamic viscosity of the base fluid are $\rho_{bf} = 1.1$ g/cm^3 and $\mu_{bf} = 0.15$ g/(cm · s), respectively. The computational domain is taken as $N_x \times N_y \times N_z = 70 \times 70 \times 210$. Zero velocity is applied at the inlet, and the normal derivative of velocity is zero at the outlet.

Fig. 3(a) shows the drag coefficient of a microparticle settling in nanofluids. The nanoparticle diameter is between 25 nm and 100 nm, and the nanoparticle volume fraction is 0.1 – 5%. It is determined that the drag coefficient increases with increasing nanoparticle volume fraction and decreasing nanoparticle diameter. To obtain a quantitative comparison of how much drag coefficient increases due to the existence of nanoparticles, we calculated the relative drag coefficient C_d^*, which is defined as

$$C_d^* = \frac{C_d - C_{d0}}{C_{d0}} \tag{20}$$

where C_{d0} is the drag coefficient of the microparticle sedimentation in the same system but without the addition of nanoparticles. It can be seen from Fig. 3(b) that a three-fold increase in the drag coefficient can be achieved by adding nanoparticles with diameter 25 nm and volume fraction 5%. It is also noted that there is a more dynamic increase in the drag coefficient for nanoparticles with smaller sizes, as nanoparticle size plays an essential role in the viscosity of nanofluids.

The above investigations of drag force for microparticle sedimentation in nanofluids takes into account of the case of a wide channel with $d_{mp}/L = 0.25$. To explore the effect of microparticle diameter to microchannel width ratio on the motion behavior of the microparticles, in the following, we compare the drag coefficient for microchannel with $d_{mp}/L = 0.25$, 0.5, and 0.75. To quantitatively describe the effects of microchannel width, we calculated the relative drag coefficient C_d^* in Eq. 20. Here, we choose C_{d0} as the drag coefficient of the microparticle sedimentation in an unconfined domain containing nanofluids. To mimic the infinite unconfined domain, a periodic boundary condition is applied in the horizontal direction, while the moving computational domain is used in the vertical direction.

It is interesting to note from Fig. 4 that decreasing the microchannel width can lead to a dramatically increase in the drag coefficient. As shown in Fig. 4, the drag coefficient can generally increase two or three orders of magnitude for the nanoparticle diameter and nanoparticle volume fraction considered. This implies that microparticle diameter to microchannel width ratio plays the most critical role in determining the drag coefficient for a microparticle sedimentation.

3.4. A single microparticle migrating in nanofluids

The phenomenon of inertial migration was first observed by Segré–Silberberg (Segre, 1961) more than fifty years ago, and had not found its practical application until the emergence of microfluidic technology (Amini et al., 2014; Di Carlo, 2009; Zhang et al., 2016). In microfluidics, both fluid inertial and viscosity are finite, which brings applications on precise manipulation of particles, including focusing and separation. In this work, we will investigate the effects of adding nanofluids in microfluidics, including nanoparticle volume fraction and nanoparticle diameter.

In the simulations, the diameters of the microparticle and the tube are $d_{mp} = 60$ μm and $D = 300$ μm, respectively. The density of the microparticle and nanoparticle are $\rho_{mp} = 3$ g/cm^3 and $\rho_{np} = 4$ g/cm^3, respectively. The density and dynamic viscosity of the base fluid are $\rho_{bf} = 1.1$ g/cm^3 and $\mu_{bf} = 0.15$ g/(cm · s), respectively. The computational domain size is 237 × 79 × 79 lattice. Pressure boundary conditions are set at the inlet and outlet. Fig. 5 shows the equilibrium position of the microparticle center off the microtube axis. The results suggest that controlling the nanoparticle volume fraction and its diameter will be an additional option on accurately separating or focusing the microparticles in microfluidics.

3.5. Mathematical correlation on relative viscosity

First, we consider a neutrally buoyant micro spherical particle in Couette flow without adding nanoparticles. Initially, the particle is put at the center of the computational domain, while the top and bottom walls are moving in opposite directions, as illustrated in Fig. 6. The relative viscosity of the flow system is defined as

$$\mu_r = \frac{\mu_s}{\mu_{bf}} = \frac{\langle \sigma \rangle}{\rho \nu G} \tag{21}$$

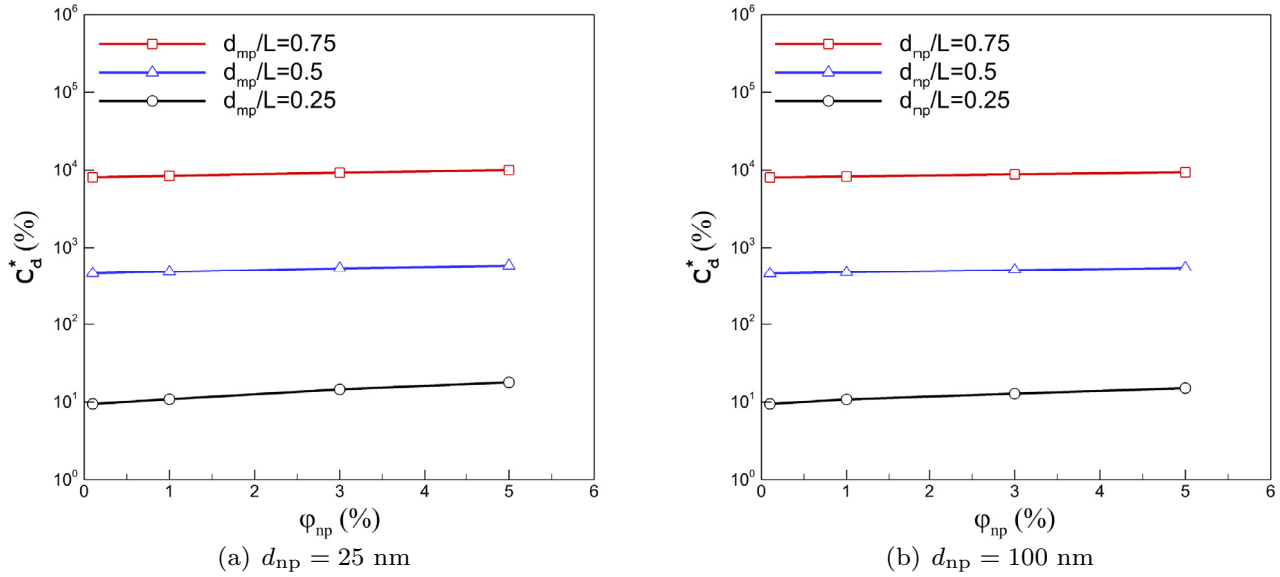

Fig. 4. Drag coefficient of a microparticle settling in nanofluids with different microchannel width.

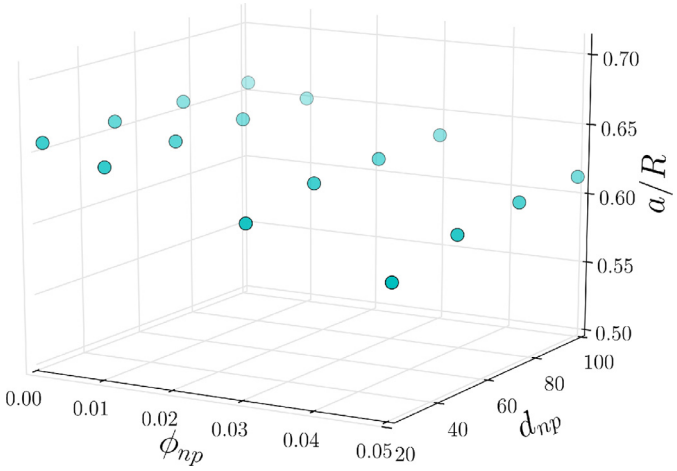

Fig. 5. Equilibrium center position of the microparticle migration in microtube filled with nanofluids.

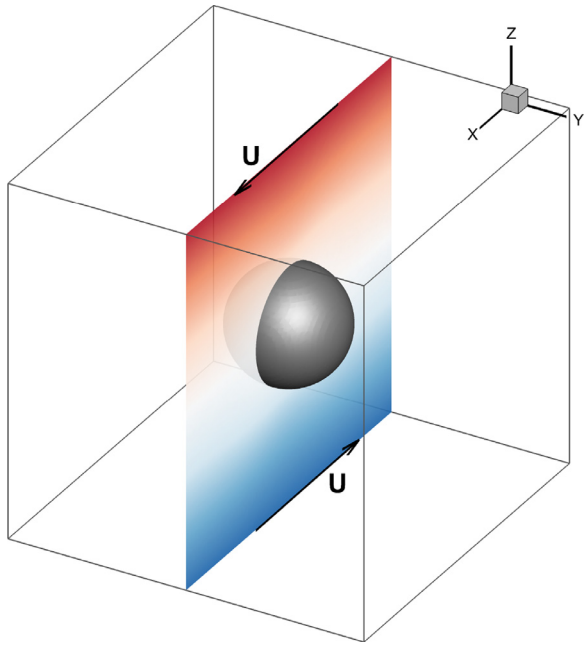

Fig. 6. Illustration of a spherical particle suspended in Couette flow, the slice shows velocity of liquid in horizontal direction.

where μ_s and μ_{bf} are the effective viscosity of suspension and viscosity of the base fluid, respectively. G is the shear rate of Couette flow without adding particles. As reported by Huang et al. (2012a); 2012b), the average shear stress $\langle\sigma\rangle$ can be obtained through averaging the shear stress acting on the moving flat wall over time.

In the simulation, the computational domain size is 120 × 120 × 120 lattice. The radius of the spherical particle is between 10 and 20 lattice, resulting in the volume fraction of solid particles between 0.24% and 1.92%. Periodical boundary conditions are applied in the X and Y directions; the upper and lower boundaries are moving solid walls. Fig. 7 shows the simulation results of relative viscosity compared with Einstein's theory of relative viscosity in dilute suspensions of spheres. It is clearly demonstrated that our adopted method is capable of calculating relative viscosity of sphere particle suspensions.

Now, we consider the viscosity of the suspensions that contain both micro- and nanoparticles. The computational domain size is 120 × 120 × 120 lattice. The radius of the microparticle is chosen as r_{mp} = 10, 12, 14, 16, 17, 18, 19, 20 lattice, which generates the microparticle volume fraction of ϕ_{mp} = 0.241%, 0.415%, 0.659%, 0.985%, 1.181%, 1.402%, 1.649%, 1.932%; the nanoparticle volume fraction is set as ϕ_{np} = 0.1%, 1%, 2%, 3%, 4%, 5%; the nanoparticle diameter is set as d_{np} = 25 nm, 50 nm, 75 nm, 100 nm. The scatter points in Fig. 8 show the calculated relative viscosities. Based on the simulation data set with 192 points, we propose a mathematic correlation between relative viscosity of suspensions and micro- and nanoparticle volume fraction, which is written as

$$\mu_r = \frac{\mu_s}{\mu_{bf}} = 1 + 3.8\phi_{mp} + 750\left(\frac{d_{np}}{d_{bf}}\right)^{-0.5}\phi_{np}^{1.57} \tag{22}$$

where μ_r denotes the relative viscosity between the suspensions and the base fluid. ϕ_{mp} and ϕ_{np} are the volume fractions of micro- and nanoparticle, respectively. d_{np} is the diameter of nanoparti-

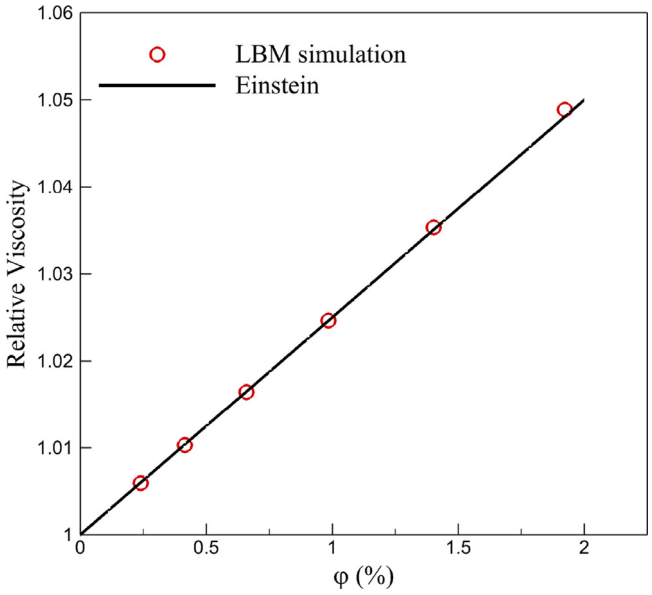

Fig. 7. Relative viscosity of the suspension as a function of particle volume fraction.

cle and $d_{bf} = 0.1\left[6M/(\pi N_A \rho_{f0})\right]^{1/3}$ is the equivalent diameter of a base fluid molecule, with M as the molecular weight of the base fluid. The adjusted R-squared value for this correlation is 0.9963, suggesting our proposed correlation fits the simulation data well.

4. Conclusion

In this work, we have presented a three-dimensional LB model to simulate suspensions that contain both micro- and nanoparticles. The microparticle dynamics is explicitly resolved, whilst the nanoparticle and base fluid are described as continua. The effects of micro- and nanoparticle volume fraction, nanoparticle diameter, and microchannel size are examined with the present model. The main findings are summarized as follows:

1. The drag coefficient for microparticle sedimentation increases with increasing nanoparticle volume fraction and decreasing nanoparticle diameter. Moreover, the drag coefficient increases faster for nanoparticles with smaller sizes.
2. The equilibrium position of the microparticle migration can be adjusted by adding nanoparticles with various volume fractions and diameters, which offers an additional option to accurately control the microparticles motion in microfluidics.
3. A mathematical correlation for predicting the relative viscosity of suspensions has been proposed, which incorporates micro- and nanoparticle volume fraction. It is believed that this correlation represents a useful engineering tool for analysis and design application.

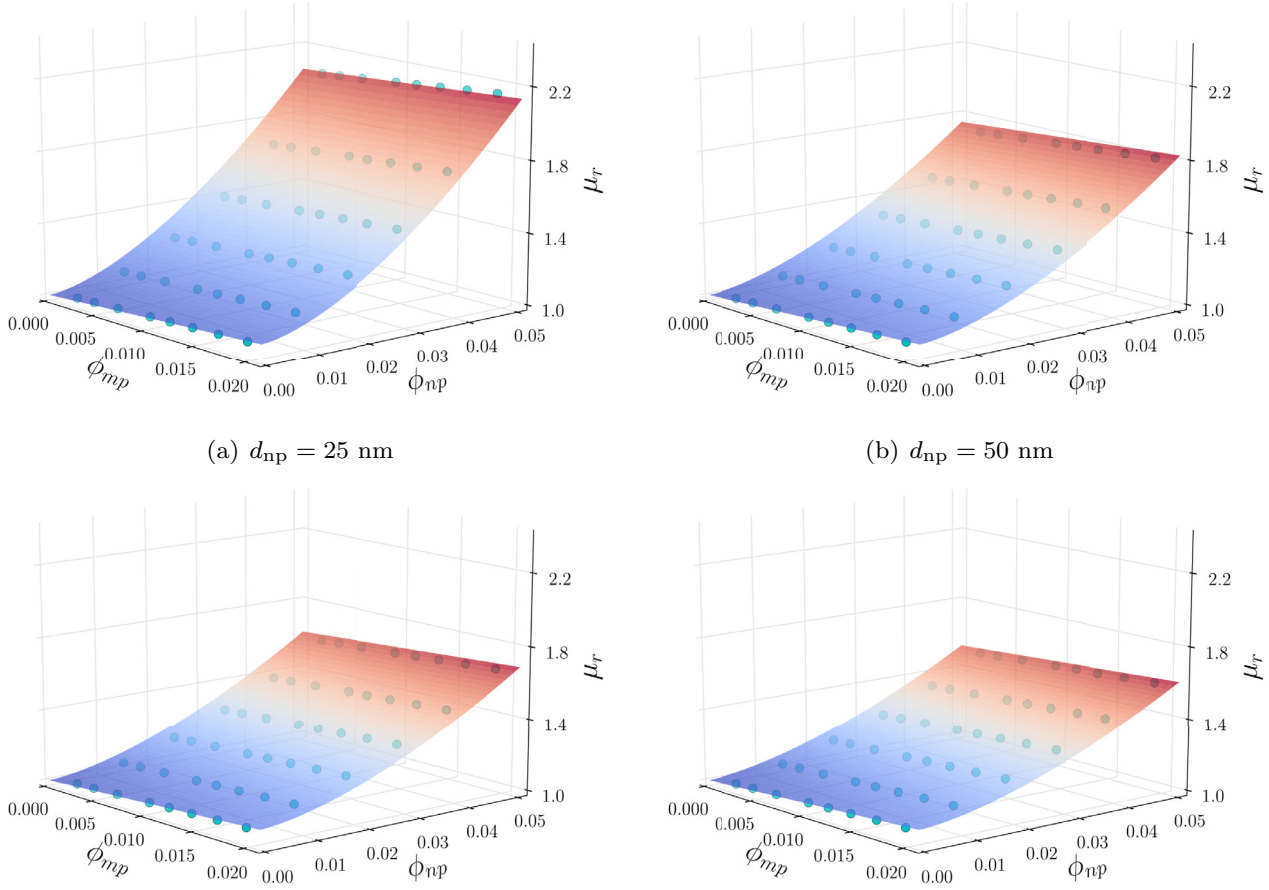

(a) $d_{np} = 25$ nm (b) $d_{np} = 50$ nm

(c) $d_{np} = 75$ nm (d) $d_{np} = 100$ nm

Fig. 8. Relative viscosity as a function of micro- and nanoparticles volume fraction.

Acknowledgement

The work described in this paper was fully supported by a grant from the Research Grants Council of the Hong Kong Special Administrative Region, China (Project No. 623313).

References

Aidun, C.K., Lu, Y., Ding, E.-J., 1998. Direct analysis of particulate suspensions with inertia using the discrete boltzmann equation. J. Fluid Mech. 373, 287–311.
Amini, H., Lee, W., Di Carlo, D., 2014. Inertial microfluidic physics. Lab Chip 14 (15), 2739–2761.
Bouzidi, M., Firdaouss, M., Lallemand, P., 2001. Momentum transfer of a boltzmann-lattice fluid with boundaries. Phys. Fluids (1994-present) 13 (11), 3452–3459.
Chen, Y., Cai, Q., Xia, Z., Wang, M., Chen, S., 2013. Momentum-exchange method in lattice boltzmann simulations of particle-fluid interactions. Phys. Rev. E 88 (1), 013303.
Corcione, M., 2011a. Empirical correlating equations for predicting the effective thermal conductivity and dynamic viscosity of nanofluids. Energy Conv. Manage. 52 (1), 789–793.
Corcione, M., 2011b. Rayleigh-bénard convection heat transfer in nanoparticle suspensions. Int. J. Heat Fluid Flow 32 (1), 65–77.
Das, S.K., Putra, N., Roetzel, W., 2003. Pool boiling characteristics of nano-fluids. Int. J. Heat Mass Transf. 46 (5), 851–862.
d'Humiéres, D., 2002. Multiple–relaxation–time lattice boltzmann models in three dimensions. Philosoph. Trans. R. Soc. London. Ser. A 360 (1792), 437–451.
Di Carlo, D., 2009. Inertial microfluidics. Lab Chip 9 (21), 3038–3046.
Feng, J., Hu, H.H., Joseph, D.D., 1994a. Direct simulation of initial value problems for the motion of solid bodies in a newtonian fluid part 1. sedimentation. J. Fluid Mech. 261, 95–134.
Feng, J., Hu, H.H., Joseph, D.D., 1994b. Direct simulation of initial value problems for the motion of solid bodies in a newtonian fluid. part 2. couette and poiseuille flows. J. Fluid Mech. 277, 271–301.
Glowinski, R., Pan, T., Hesla, T., Joseph, D., Periaux, J., 2001. A fictitious domain approach to the direct numerical simulation of incompressible viscous flow past moving rigid bodies: application to particulate flow. J. Comput. Phys. 169 (2), 363–426.
Hatzell, K.B., Boota, M., Gogotsi, Y., 2015. Materials for suspension (semi-solid) electrodes for energy and water technologies. Chem. Soci. Rev. 44 (23), 8664–8687.
He, Y., Jin, Y., Chen, H., Ding, Y., Cang, D., Lu, H., 2007. Heat transfer and flow behaviour of aqueous suspensions of tio2 nanoparticles (nanofluids) flowing upward through a vertical pipe. Int. J. Heat Mass Transf. 50 (11), 2272–2281.
Van der Hoef, M., van Sint Annaland, M., Deen, N., Kuipers, J., 2008. Numerical simulation of dense gas-solid fluidized beds: A multiscale modeling strategy. Ann. Rev. Fluid Mech. 40, 47–70.
Huang, H., Wu, Y., Lu, X., 2012a. Shear viscosity of dilute suspensions of ellipsoidal particles with a lattice boltzmann method. Phys. Rev. E 86 (4), 046305.
Huang, H., Yang, X., Krafczyk, M., Lu, X.-Y., 2012b. Rotation of spheroidal particles in couette flows. J. Fluid Mech. 692, 369–394.
Huang, H., Yang, X., Lu, X.-Y., 2014. Sedimentation of an ellipsoidal particle in narrow tubes. Phys. Fluids (1994-present) 26 (5), 053302.
Jebakumar, A.S., Premnath, K.N., Abraham, J., 2016. Lattice boltzmann method simulations of stokes number effects on particle trajectories in a wall-bounded flow. Comput. Fluids 124, 208–219.
Ladd, A.J., 1994. Numerical simulations of particulate suspensions via a discretized boltzmann equation. part 1. theoretical foundation. J. Fluid Mech. 271 (1), 285–309.
Lallemand, P., Luo, L.-S., 2000. Theory of the lattice boltzmann method: Dispersion, dissipation, isotropy, galilean invariance, and stability. Phys. Rev. E 61 (6), 6546.
Lallemand, P., Luo, L.-S., 2003. Lattice boltzmann method for moving boundaries. J. Comput. Phys. 184 (2), 406–421.
Lee, J.-H., Hwang, K.S., 2008. Effective viscosities and thermal conductivities of aqueous nanofluids containing low volume concentrations of al2o3 nanoparticles. Int. J. Heat Mass Transf. 51 (11), 2651–2656.
Lishchuk, S., Halliday, I., Care, C., 2006. Shear viscosity of bulk suspensions at low reynolds number with the three-dimensional lattice boltzmann method. Phys. Rev. E 74 (1), 017701.
Maiga, S.E.B., Palm, S.J., Nguyen, C.T., Roy, G., Galanis, N., 2005. Heat transfer enhancement by using nanofluids in forced convection flows. Int. J. Heat Fluid Flow 26 (4), 530–546.
Miyamura, A., Iwasaki, S., Ishii, T., 1981. Experimental wall correction factors of single solid spheres in triangular and square cylinders, and parallel plates. Int. J. Multiph. Flow 7 (1), 41–46.
Oztop, H.F., Abu-Nada, E., 2008. Numerical study of natural convection in partially heated rectangular enclosures filled with nanofluids. Int. J. Heat Fluid Flow 29 (5), 1326–1336.
Peng, C., Teng, Y., Hwang, B., Guo, Z., Wang, L.-P., 2016. Implementation issues and benchmarking of lattice boltzmann method for moving rigid particle simulations in a viscous flow. Comput. Math. Appl. 72 (2), 349–374.
Peskin, C.S., 1977. Numerical analysis of blood flow in the heart. J. Comput. Phys. 25 (3), 220–252.
Qian, Y., d'Humiéres, D., Lallemand, P., 1992. Lattice bgk models for navier-stokes equation. EPL (Europhys. Lett.) 17 (6), 479.
Segre, G., 1961. Radial particle displacements in poiseuille flow of suspensions. Nature 189, 209–210.
Tao, S., Hu, J., Guo, Z., 2016. An investigation on momentum exchange methods and refilling algorithms for lattice boltzmann simulation of particulate flows. Comput. Fluids 133, 1–14.
Tenneti, S., Subramaniam, S., 2014. Particle-resolved direct numerical simulation for gas-solid flow model development. Ann. Rev. Fluid Mech. 46, 199–230.
Yang, B., Wang, J., Joseph, D., Hu, H.H., Pan, T.-W., Glowinski, R., 2005. Migration of a sphere in tube flow. J. Fluid Mech. 540, 109–131.
Yang, K., Guo, Z., 2016. Lattice boltzmann study of wettability alteration in the displacement of nanoparticle-filled binary fluids. Comput. Fluids 124, 157–169.
Yang, X., Huang, H., Lu, X.-Y., 2015. Sedimentation of an oblate ellipsoid in narrow tubes. Phys. Rev. E 92 (6), 063009.
Zarghami, A., Ubertini, S., Succi, S., 2013. Finite-volume lattice boltzmann modeling of thermal transport in nanofluids. Comput. Fluids 77, 56–65.
Zhang, J., Yan, S., Yuan, D., Alici, G., Nguyen, N.-T., Warkiani, M.E., Li, W., 2016. Fundamentals and applications of inertial microfluidics: a review. Lab Chip 16 (1), 10–34.